

OPTICAL DESIGN OF COATLI: A DIFFRACTION-LIMITED VISIBLE IMAGER WITH FAST GUIDING AND ACTIVE OPTICS CORRECTION

J. Fuentes-Fernández, S. Cuevas, and A. M. Watson

Instituto de Astronomía, UNAM, México

Received January 13 2017; accepted August 31 2017

ABSTRACT

We present the optical design of COATLI, a two channel visible imager for a commercial 50 cm robotic telescope. COATLI will deliver diffraction-limited images (approximately 0.3 arcsec FWHM) in the *riz* bands, inside a 4.2 arcmin field, and seeing limited images (approximately 0.6 arcsec FWHM) in the *B* and *g* bands, inside a 5 arcmin field, by means of a tip-tilt mirror for fast guiding, and a deformable mirror for active optics, both located on two optically transferred pupil planes. The optical design is based on two collimator-camera systems plus a pupil transfer relay, using achromatic doublets of CaF₂ and S-FTM16 and one triplet of N-BK7 and CaF₂. We discuss the efficiency, tolerancing, thermal behavior and ghosts. COATLI will be installed at the Observatorio Astronómico Nacional in Sierra San Pedro Mártir, Baja California, Mexico, in 2018.

RESUMEN

Presentamos el diseño óptico de COATLI, una cámara visible de dos canales para un telescopio comercial robótico de 50 cm. COATLI producirá imágenes al límite de difracción (0.3 arcsec FWHM aproximadamente) en las bandas *riz*, e imágenes al límite de *seeing* (0.6 arcsec FWHM aproximadamente) en las bandas *B* y *g*, usando un espejo articulado para guiado rápido y un espejo deformable para óptica activa, ambos situados en dos planos de pupila. El diseño óptico está basado en dos sistemas colimador-cámara y un sistema de transferencia de pupila, usando dobletes acromáticos de CaF₂ y S-FTM16 y un triplete de N-BK7 y CaF₂. Discutimos la eficiencia final, tolerancias, comportamiento térmico y fantasmas. COATLI se instalará en el Observatorio Astronómico Nacional en Sierra San Pedro Mártir, Baja California, México, en 2018.

Key Words: instrumentation: adaptive optics — telescopes

1. INTRODUCTION

COATLI will produce images with FWHM of approximately 0.3 arcsec in a field of view (FoV) larger than 4 arcmin over a large fraction of the sky from 550 nm to 920 nm, from the Observatorio Astronómico Nacional (OAN) in Sierra San Pedro Mártir (SPM). The site has seeing values similar to the sites in Hawaii, Chile and the Canary Islands, with an average value of 0.79 arcsec FWHM at 500 nm and a corresponding value of the Fried parameter of 13 cm (Skidmore 2009). By using a combination of fast guiding and active optics, COATLI will be able to obtain images better than the excellent seeing, even in relatively poor atmospheric conditions. The one drawback of the instrument is that

the telescope will be relatively small (50 cm), which will limit us to science on relatively bright sources. We estimate 10σ limiting magnitudes in dark/bright time of 23.8/23.4 in *r*, 23.3/22.9 in *i*, and 22.6/22.3 in *z* in 1000 seconds.

As have been exposed in Watson et al. (2016), examples of scientific cases for COATLI can be eclipsing binaries in the Trapezium, HII regions in nearby galaxies, galactic star clusters, location of gamma-ray bursts in their host galaxies, sub-stellar companions in the solar neighborhood, multiplicity in young clusters, and planetary nebulae in the galactic bulge.

The telescope and instrument COATLI were conceived from the fact that if a telescope diameter is less than 3.3 times the Fried parameter, fast guiding

or tip-tilt correction can reduce the phase variance to less than 1 rad^2 and hence produce diffraction-limited images (Watson et al. 2016). Theoretically, at the OAN/SPM one could then obtain diffraction-limited images at 500 nm with a 50 cm telescope with fast guiding only. However, in order to deliver this image quality, the static image quality of the telescope and instrument must also be diffraction-limited.

The telescope selected for COATLI is a commercial 50 cm f/8 Ritchey-Chrétien from the company ASTELCO on a German mount. By design, a Ritchey-Chrétien is free of spherical aberration and coma. Nevertheless, telescope misalignments can introduce static aberrations of these two types: spherical aberration caused by errors in the distance between the two mirrors and constant coma caused by tilts and misalignments in any of the mirrors (Wilson 2004). Additionally, irregularities in mirror polishing and mechanical support of the mirrors will introduce astigmatism in the beam. In practice, though, spherical aberration is not a problem, provided the instrument focal plane is close to the telescope focal plane. Therefore, the active optics system will have to correct both static astigmatism and constant coma.

COATLI will do fast guiding using a tip-tilt mirror and active optics correction using a deformable mirror. The deformable mirror is an Adaptica Saturn 48-element push-pull electrostatic mirror. The instrument does not have a wavefront sensor; hence, the aberrations will be detected and measured using the *donut* method (Tokovinin and Heathcote 2006), which consists of fitting a model of a defocused aberrated beam to an out-of-focus image on the detector. The required defocus will be introduced by the deformable mirror.

In this paper, we present the novelty of the optical design of the instrument and the details of it. In § 2 we present and justify the design architecture; in § 3 we put the optical design of COATLI in a wider context and present a comparison to designs of similar astronomical instruments; in § 4 we present the requirements of the instrument with its nominal image quality and efficiency; in § 5 we discuss the telescope’s aberrations and the active optics correction; in § 6 we discuss the tolerancing of the instrument; in § 7 we present a brief discussion on thermal behavior and ghosts; in § 8 we present the possibility of using the *B* band for additional science; and we finish with some conclusions in § 9.

2. DESIGN ARCHITECTURE

COATLI will have two channels, one with an EMCCD for tip-tilt correction, namely the blue channel, and one with a standard CCD to avoid excess Poisson noise, namely the red channel. The blue channel will observe at the seeing limit in the *g* band (from 400 to 550 nm) and the red channel will observe at the diffraction limit in the *riz* bands (from 550 to 920 nm).

There are several considerations which guide the design architecture. Firstly, the deformable mirror shall be located in a pupil plane, and the blue and red channels shall be separated with a dichroic before the deformable mirror, because its reflectivity in the blue part of the spectrum is not good. Secondly, the tip-tilt mirror shall be located before the dichroic in order for the fast guiding system to work in close loop at the blue channel. And thirdly, the tip-tilt mirror shall be located at another pupil plane, since otherwise it would shift the image of the telescope’s secondary mirror over the deformable mirror, potentially laying out of its small active surface (10.8 mm in diameter). In addition, placing the dichroic in a collimated beam avoids the introduction of asymmetric aberrations to the red channel.

Therefore, the system needs a collimator system common to both the blue and red channels, a pupil transfer relay that conjugates the pupil image from the tip-tilt to the deformable mirror, and two independent camera systems for the two channels. The blue detector is an *Andor Ixon* EMCCD with 1024×1024 13 μm pixels and the red detector is an *Andor Ikon* CCD with 2048×2048 13.5 μm pixels.

The two detectors are located approximately on the same side of the telescope, opposite the German mount. The optical design is based on several achromatic lens doublets and one lens triplet for the red camera. The use of lenses as opposed to mirrors is convenient because the instrument needs to be very compact and because it is a visible instrument. The optical layout of COATLI is shown in Figures 1 and 2. Light from the telescope enters the instrument through an entrance window (1) towards a fold mirror (2) which bends the beam in a direction perpendicular to the optical axis of the telescope; the collimator (3), common for the two channels, is an achromat doublet that sends the beam towards the tilt mirror (4), located at a pupil plane; the dichroic (5) then splits the beam at 550 nm, transmitting the red channel and reflecting the blue channel downwards. Blue light is then bent with another fold mirror (6) towards the blue camera (7), an achromatic doublet with a small telephoto effect; blue filters (8)

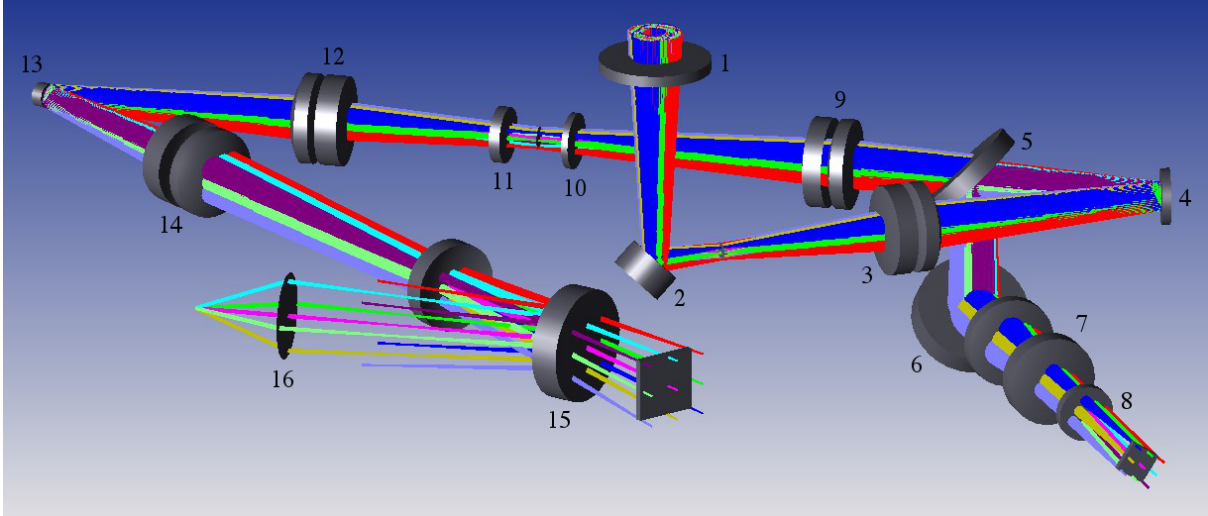


Fig. 1. 3D layout of COATLI. The optical components of the instrument are numbered as follows. 1: entrance window (EW); 2: common path fold mirror (CFM); 3: collimator (COL); 4: tip-tilt mirror (TM); 5: dichroic (DIC); 6: blue channel fold mirror (BFM); 7: blue channel camera (BCAM); 8: blue channel filter (BF); 9/12: pupil relay (REL); 10/11: red channel filters (RF); 13: deformable mirror (DM); 14: red channel triplet camera (RCAM); 15: beam splitter (BS); and 16: pupil camera (PCAM). The color figure can be viewed online.

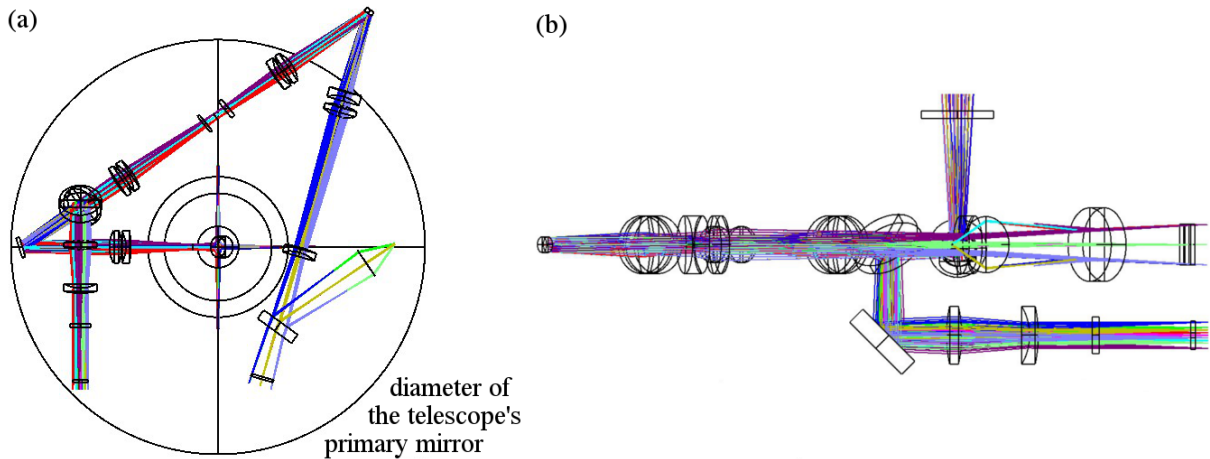


Fig. 2. 2D layout of COATLI, where (a) shows a bottom view along the azimuthal axis and (b) shows a lateral view along the axis of the collimator.

are located in one wheel between the camera and the detector. Red light passes through the dichroic towards the pupil transfer relay, which is formed by two non-identical achromatic doublets (9 and 13); the red filters (10 and 11) are located in two separate wheels before and after the focal plane that lies in the relay; the deformable mirror (13) is located at a second pupil plane, and this sends the light towards the red camera (14), a telephoto triplet. The maximum sizes of the two pupil images are 13.0 mm and

10.7 mm for the pupil images on the tip-tilt mirror and on the deformable mirror, respectively.

Right before the red detector, there is a beam splitter (15) the first surface of which is uncoated and reflects 4% of the light towards a commercial Tamron 12VM1040ASIR lens (16) which produces an image of the pupil on a CMOS UI-1220-M-GL detector; this pupil camera is used for diagnostic and alignment purposes. The second surface of the beam splitter is coated in order to reduce the intensity of the pupil

TABLE 1
OPTICAL PRESCRIPTION FOR THE LENSES OF COATLI

Lens	Material	D	R_1	R_2	FL	CT
COL1	S-FTM16	40	100.608 cx	40.000 cc	-112.675	6.0
COL2	CaF ₂	40	56.671 cx	40.000 cx	54.167	15.1
BCAM1	CaF ₂	40	92.493 cx	95.011 cx	108.264	10.4
BCAM2	S-FTM16	40	41.473 cc	100.32 cx	-119.975	6.0
REL1	CaF ₂	40	93.429 cx	49.591 cx	74.834	12.4
REL2	S-FTM16	40	40.000 cc	69.914 cx	-158.640	6.0
REL3	S-FTM16	40	137.918 cx	40.000 cc	-95.605	6.0
REL4	CaF ₂	40	56.4254 cx	40.000 cx	54.069	15.1
RCAM1	N-BK7	40	200.203 cc	40.000 cc	-64.723	6.0
RCAM2	CaF ₂	40	71.604 cx	40.000 cx	59.283	14.3
RCAM3	N-BK7	40	111.771 cx	41.564 cc	-128.462	6.0

ghost and increase the efficiency in the red channel. In addition, the inclination and thickness of the beam splitter have been chosen so that the pupil image and its ghost do not overlap on the CMOS detector. The pupil image has a diameter of 0.86 mm or 140 pixels on the detector.

All lens groups except for the red camera (excluding the pupil camera lens, which is a commercial component) are non-cemented doublets of calcium fluoride (CaF₂) and Ohara S-FTM16 (Brown et al. 2004). The optics workshop of the IA-UNAM (Instituto de Astronomía - Universidad Nacional Autónoma de México) has experience in polishing the two materials for the near infrared instrument FRIDA (Cuevas et al. 2006). The red camera telephoto is N-BK7/CaF₂/N-BK7 triplet. This group on its own produces a relatively high axial chromatic shift, however the red camera is not strongly powered and the chromatic shift induced by it is opposite to the residual chromatism left by all the previous optics. This leaves the red channel nearly apochromatic. No aspheric surfaces are present in the design, which will allow all the lenses to be manufactured in the optical workshops of the Instituto de Astronomía of the Universidad Nacional Autónoma de México (IA-UNAM). Table 1 shows the optical prescriptions of all the lenses of COATLI, where D is diameter, R is curvature radius, FL is focal length and CT is center thickness. Negative and positive focal lengths indicate divergent/convergent lenses and all units are millimeters.

There are three FLI CFW1 filter wheels each with eight holes for filters of 25 mm diameter: one in the blue channel, before the detector, with filters

5 mm thick; and two in the red channel, between the pupil transfer relay, with filters 3 mm and 5 mm thick respectively. The two red filter wheels will have one clear filter each to avoid the need to refocus when using one or the other.

3. COMPARISON TO OTHER ASTRONOMICAL INSTRUMENTS

The novelty of the design lies in the fact that the instrument needs to deliver diffraction-limited images in the visible, in a wide FoV and a relatively broad spectral range. To our knowledge, no similar design has ever been reported. Other astronomical instruments with adaptive optics (AO) usually work in the near infrared and have a smaller corrected field. (Although, for large telescopes, this may be equivalent in terms of the number of Airy discs within the field). Typically, these instruments use mirrors for their powered optics to avoid chromatic aberration, and have only one or none pupil planes, which simplifies enormously the optical design. Examples of these are PUEO at the CFHT (Arsenault et al. 1994), NAOS at the VLT (Rousset et al. 1998), the Lick AO system (Gavel et al. 2000), or PHARO at Palomar (Hayward et al. 2001), to mention a few. FRIDA, the future AO instrument for the GTC (Cuevas et al. 2006), has demonstrated the excellent performance of achromatic lens systems for a diffraction-limited instrument, for an equivalent FoV (40 arcsec in a 10.4 m telescope vs 4 arcmin in a 0.5 m telescope, with the same amount of pixels on the detector, and both instrument being Nyquist sampled), but as the previous, FRIDA will work in the near infrared. In contrast, VisAO for

TABLE 2
HIGH LEVEL REQUIREMENTS OF COATLI

Channel	Wavelength (nm)	FoV (arcmin)	Scale (arcsec/px)	Image quality
blue	400 - 550	diam ≥ 4	0.250 - 0.350	$d_{80}^{I+S}/d_{80}^{D+S} \leq 1.25$ (goal: 1.10)
red	550 - 922	diam ≥ 4	0.100 - 0.125	$SR \geq 0.7$ (goal: 0.8)

the Magellan Clay telescope (Kopon et al. 2010) is an example of an AO instrument in the visible, in a 6.5 m telescope. However, this is a direct imaging instrument with almost no optics, since the telescope’s secondary mirror acts as the adaptive element, which provides a very small corrected FoV of 8.4 arcsec.

4. REQUIREMENTS AND NOMINAL PERFORMANCE

4.1. Instrument Requirements

The high level requirements of COATLI are summarized in Table 2. The image quality in the blue channel is given in terms of the ratio of the d_{80} (this is the standard definition of the diameter that contains 80% of the energy from the image of a point source) of the instrument with the atmospheric contribution and the seeing limited case, and shall be lower than 1.25 (with a goal of better than 1.10). In the red channel, the Strehl Ratio shall be at least 0.7 (with a goal of better than 0.8). The field of view (FoV) of the two channels shall be at least 4 arcmin in diameter, and the plate scale shall be between 0.25 and 0.35 arcsec in the blue channel, and between 0.100 and 0.125 arcsec per pixel in the red channel.

The requirements in FoV are specified for an appropriate coverage of the isokinetic angle, which is expected to be about 2 arcmin (Watson et al. 2016). The plate scales are specified with an upper limit given by the need to sample at the seeing limit in the blue channel, and to sample the best expected images of 0.25 arcsec FWHM in the red channel. The lower limits are to reduce the contribution of the detector noise when oversampling.

The requirements for image quality are given in terms of the Strehl Ratio (SR) and the d_{80} ratio. The superscripts D , S and I correspond to the contributions of diffraction, seeing and the instrument’s optics including the telescope, respectively, so that d_{80}^I is the value delivered by the instrument without the atmosphere, d_{80}^D is the value for a non-aberrated system (diffraction limited) and d_{80}^S is the contribution of the atmosphere. In this way, d_{80}^{I+S} and

d_{80}^{D+S} are the quadratically added values from the instrument with the atmosphere and from the non-aberrated system with the atmosphere (Watson et al. 2016).

4.2. Nominal Performance

Nominal performance refers to the instrument as designed, without taking into account tolerancing or thermal effects. The nominal scales are 0.29 arcsec/px at the blue detector and 0.12 arcsec/px at the red detector, with fields of view of 5×5 arcmin and 4.2×4.2 arcmin respectively. The respective working f ratios are $f/18.2$ and $f/45$. The spot diagrams for the broad bands g in the blue channel and riz in the red channel are shown in Figure 3. The nominal image quality for the red and blue channels is shown in Figure 4, following the criteria established in Table 2. In principle, there is no need for focus adjustment at the red detector for the different filters. However, in case of this being necessary, it can be done using the deformable mirror. From Figures 3 and 4, we see that the optical quality of the instrument is well within the requirements from § 4.1. Bands *griz* achieve the requirements and goals from Table 2 in the whole area of the detector. The red channel is clearly diffraction limited. For the blue channel, assuming that the seeing scales with the value of d_{80} , with a seeing of 0.6 arcsec we get a FWHM better than 0.63 arcsec in the g band.

The focusing of COATLI will be done as follows. The blue channel will be focused using the secondary mirror and the red channel will use the deformable mirror.

4.3. Efficiency

Filters and the dichroic are provided by Custom Scientific, as well as anti-reflecting coatings for all the lenses and the second surface of the beam splitter for the pupil camera. Given the relatively short wavelength range, transmissivity will be at least 99% per surface per lens. The requirements of COATLI define that the mean efficiency shall be greater than 35%, 35%, 25% and 15% respectively in the *griz*

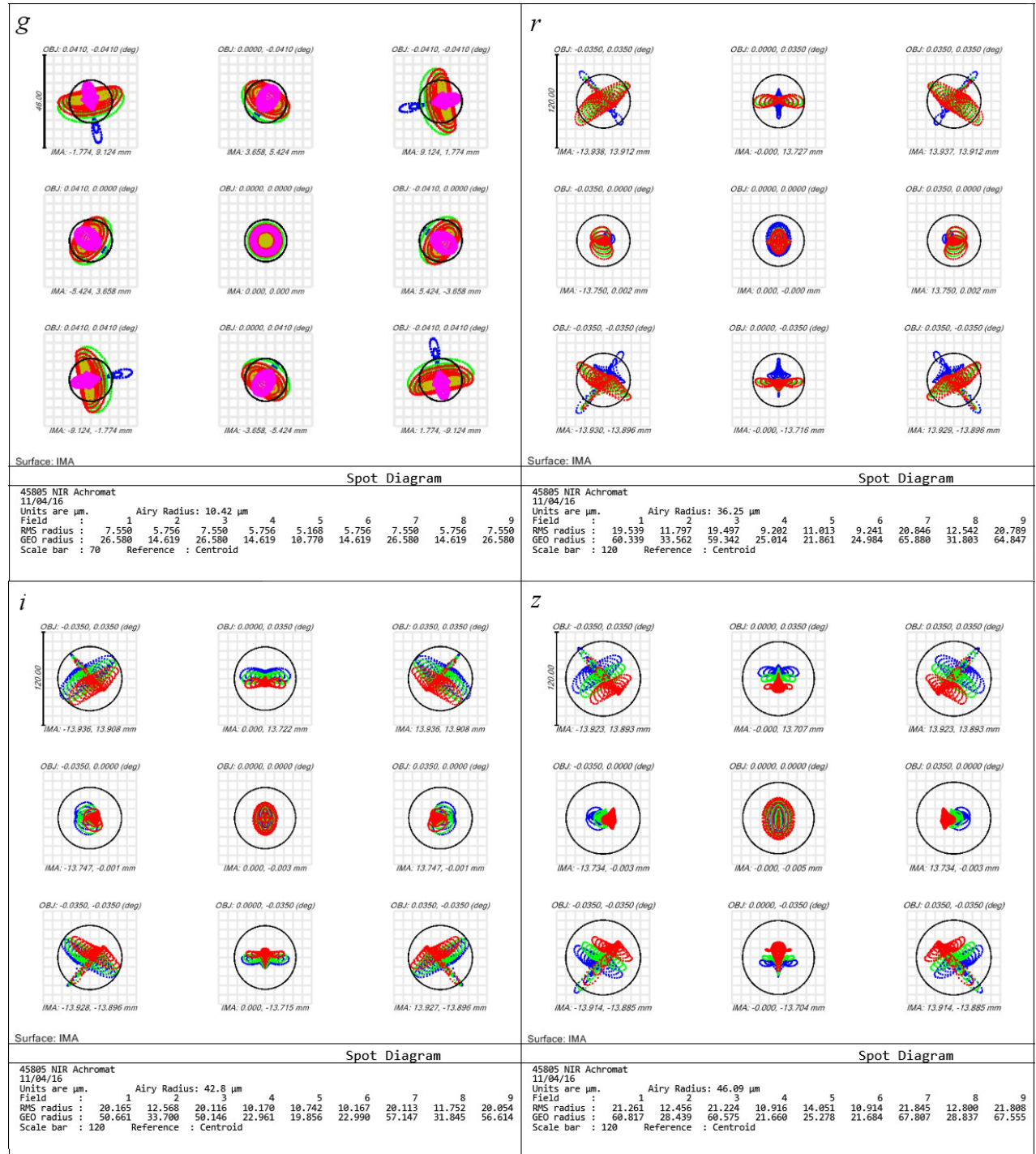


Fig. 3. Spot diagram for the blue and red channels (above and below, respectively). We show the spot diagram for the g band filter in the blue channel, and the riz bands filters for the red channel. Diagrams for the center, edges and corners of the detector are shown. The circle is the Airy disk for a central wavelength in each band. The square grid has a size of 1 arcsec in all cases. The color figure can be viewed online.

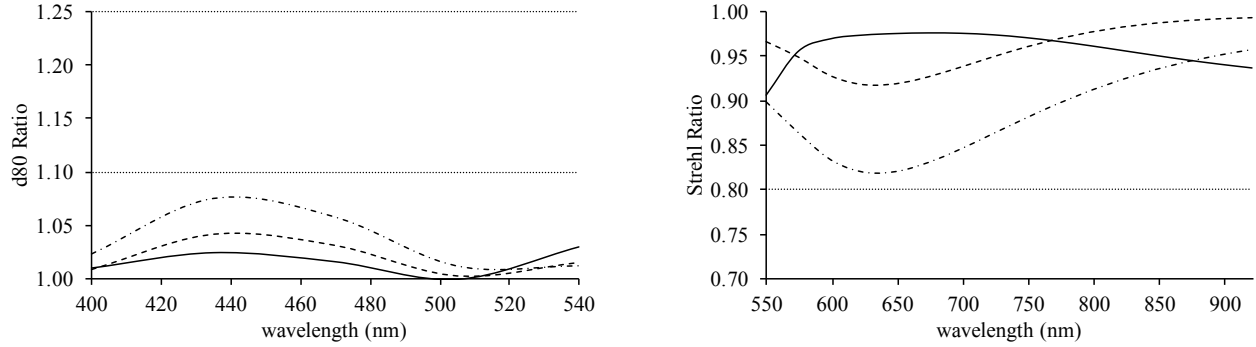


Fig. 4. Image quality of the nominal design in the blue (left) and right (right) channels, following the criteria established in Table 2. We show the values at the center of the detector (solid), at the edge (dashed) and at the corners (dot-dashed).

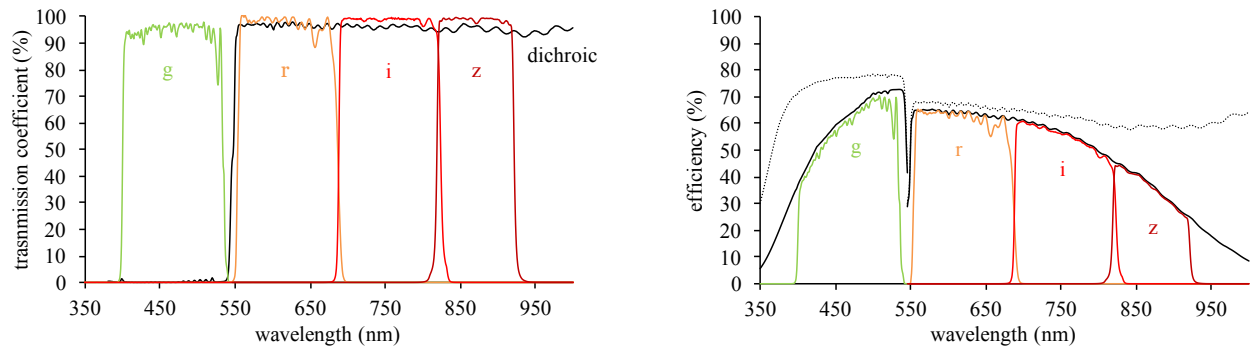


Fig. 5. Transmission coefficient of the *griz* filters and the dichroic of COATLI (left) and efficiency estimation for the blue and red channels (right). In the right plot, we show the efficiency of the telescope and instrument without filters nor detectors (black dotted), without filters but with detectors (black solid) and with filters *griz* and detectors (color solid). The color figure can be viewed online.

bands, excluding only the atmosphere and the central obturation of the telescope. The transmission curves for the five broad band filters and dichroic, and the estimated total efficiency for the two channels of COATLI are shown in Figure 5. This efficiency estimate takes account of the telescope, all the optics with coatings (lenses, mirrors, windows and filters) and the detectors.

5. ACTIVE OPTICS CORRECTION

The deformable mirror, located at the second pupil plane in the red channel path, will be able to correct for focus, astigmatism and coma. The aberrations will be measured using the *donut* method (Tokovinin and Heathcote 2006), which consists of fitting a model of a defocused aberrated beam to an out-of-focus image on the detector. The deformable mirror itself will be able to produce the desired defocus. The stroke of the deformable mirror corresponding to defocus, astigmatism and coma was measured at the facilities of the IA-UNAM, using a Zygo GPI-

6" Fizeau laser interferometer, applying a modal deformation of the mirror's actuators. Table 3 shows the values of the Zernike coefficients corresponding to the maximum stroke of the deformable mirror for defocus, astigmatism and coma, at a voltage of 240 V. Astigmatism can be applied independently from coma and defocus, since it uses the outer electrodes of the deformable mirror. Coma and defocus have to be applied sharing the inner electrodes of the deformable mirror.

Figure 6 shows the Zernike coefficients Z_5 and Z_8 (representative for astigmatism and coma) in wavefront error (WFE) RMS on the deformable mirror induced by astigmatism (Z_5) on the surfaces of the telescope's primary mirror (M1) and secondary mirror (M2) and misalignments of M2. As an example, we could correct a maximum of 254 nm of Z_5 RMS on M1, or a maximum of 325 nm of Z_5 RMS on M2, or a combination of the two; and a maximum of 1.1 mm of misalignment of M2 (assuming no focus correction).

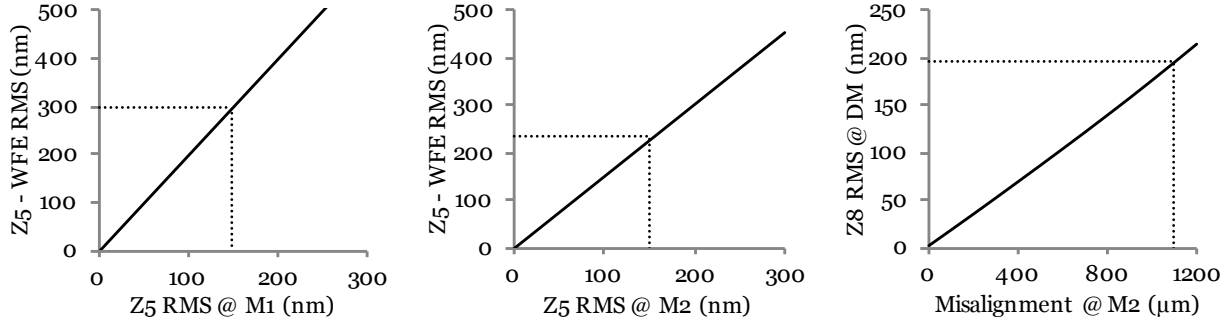


Fig. 6. Deformations on the deformable mirror in terms of the Zernike coefficients Z5 and Z8, induced by astigmatism in the telescope’s secondary mirror (left), astigmatism in the telescope’s primary mirror (center) and misalignment of the secondary mirror (right).

TABLE 3
ZERNIKE COEFFICIENTS AT THE
DEFORMABLE MIRROR

Coefficient	Mode	DM stroke (nm RMS)
Z4	defocus	1352
Z5	astigmatism	508
Z6	astigmatism	503
Z7	coma	204
Z8	coma	187

6. TOLERANCING

The tolerancing study was made through 200 Monte Carlo simulations where all the relevant optical and optomechanical parameters were varied following a parabolic statistic within a given range, specified individually for each parameter. The range for some of the parameters is given by the manufacturer, some others depend on the capabilities of the workshops and laboratories at the IA-UNAM, some parameters are more sensitive than others, etc. Also, some of the tolerances come from, or induce, restrictions in the optomechanics, which has also been designed at the IA-UNAM, and will be manufactured in our mechanics workshops. The rest of the parameters are either restrictions of the optics workshops at the IA-UNAM (such as tolerances in radius and thicknesses of the lenses), of the laboratory measurement procedures (such as tolerances in parallelism and surface irregularity), or have been evaluated in order not to degrade image quality below specifications.

The tolerances are shown in Table 4. In the table, from left to right, we show the tolerances in: refractive index (n), curvature radius of each surface of

the lens (r), thickness (t), position along the optical axis (z), decentering (Δy), inclination (α), surface inclination or parallelism (p) and surface irregularity (irr). The table is divided in three sections, the first corresponding to the lens parameters, the second to mirrors and the third to windows, filters and/or plates. The labels COL1+2, BCAM1+2, REL1+2, REL3+4 and RCAM1+2+3 refer to groups of lenses in their optomechanical barrel. The parameters with a dagger superscript are tolerances specified by an external manufacturer. While tolerances in some parameters are more restrictive in some elements than in others, when the difference is small we have maintained the more restrictive value for all the equivalent elements.

The tolerances in tilt and misalignment of the optical components are compatible with the optomechanical design (Cuevas et al. 2016).

The tolerancing study uses two types of static compensators. In the blue channel we compensate with the position of the focal plane, and in the red channel we compensate with the position and the inclination of the focal plane. From the Monte Carlo simulations mentioned above, the maximum defocus in 90% of the cases was ± 3 mm for the blue detector and ± 20 mm for the red detector, with a maximum inclination of $\pm 7^\circ$ at the red detector. To compensate the defocus in the two channels, we have left the mechanical distance between the last two lenses of each camera free within a certain adjustment, so these distances will only be fixed when we have manufactured all the optics and we know their dimensional parameters such as curvature radii and thicknesses. According to the defocus obtained by the tolerancing study, these two distances will be left to adjustment within ± 1.5 mm for the blue channel and ± 5 mm for the red channel. Further fine tuning of the detector focus and tilt (in case of the red detec-

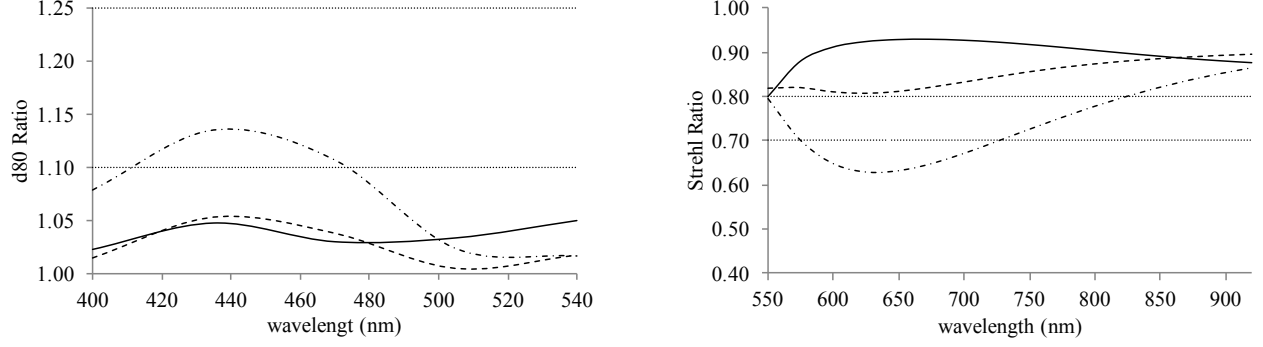


Fig. 7. Image quality in the red (left) and blue (right) channels, including tolerances, following the criteria established in Table 2. We show the values at the center of the detector (solid), at the edge (dashed) and at the corners (dot-dashed). In the blue channel, we show the g band (400-540 nm) and the B band (370-510 nm), refocusing with M2 for the latter.

TABLE 4

SUMMARY OF THE TOLERANCES OF THE INSTRUMENT

Element	n	r (mm)	t (mm)	z (mm)	Δy (mm)	α ($^\circ$)	p ($^\circ$)	irr (fringes)
COL1	$\pm 5 \times 10^{-5} \dagger$	± 0.10	± 0.10	± 0.10	± 0.03	± 0.04	± 0.03	± 1
COL2	$\pm 5 \times 10^{-5} \dagger$	± 0.10	± 0.10	± 0.05	± 0.03	± 0.04	± 0.03	± 1
COL1+2					± 0.10	± 0.10		
BCAM1	$\pm 5 \times 10^{-5} \dagger$	± 0.10	± 0.10	± 0.10	± 0.03	± 0.04	± 0.03	± 1
BCAM2	$\pm 5 \times 10^{-5} \dagger$	± 0.10	± 0.10	± 0.05	± 0.03	± 0.04	± 0.03	± 1
BCAM1+2					± 0.10	± 0.10		
REL1	$\pm 5 \times 10^{-5} \dagger$	± 0.10	± 0.10	± 0.10	± 0.03	± 0.04	± 0.03	± 1
REL2	$\pm 5 \times 10^{-5} \dagger$	± 0.10	± 0.10	± 0.05	± 0.03	± 0.04	± 0.03	± 1
REL1+2					± 0.10	± 0.10		
REL3	$\pm 5 \times 10^{-5} \dagger$	± 0.10	± 0.10	± 0.10	± 0.03	± 0.04	± 0.03	± 1
REL4	$\pm 5 \times 10^{-5} \dagger$	± 0.10	± 0.10	± 0.05	± 0.03	± 0.04	± 0.03	± 1
REL3+4					± 0.10	± 0.10		
RCAM1	$\pm 5 \times 10^{-5} \dagger$	± 0.10	± 0.10	± 0.10	± 0.03	± 0.04	± 0.03	± 1
RCAM2	$\pm 5 \times 10^{-5} \dagger$	± 0.10	± 0.10	± 0.05	± 0.03	± 0.04	± 0.03	± 1
RCAM3	$\pm 5 \times 10^{-5} \dagger$	± 0.10	± 0.10	± 0.10	± 0.10	± 0.10	± 0.03	± 1
RCAM1+2+3					± 0.10	± 0.10		
CFM				± 0.05		± 0.10		$\pm 0.10 \dagger$
TM				± 0.50		± 0.10		$\pm 0.20 \dagger$
BFM				± 0.50		± 0.10		$\pm 0.10 \dagger$
DM				± 0.50		± 0.10		
EW			$\pm 0.10 \dagger$	± 1.00		± 1.00	$\pm 0.002 \dagger$	$\pm 0.20 \dagger$
DIC			$\pm 0.10 \dagger$	± 0.50		± 1.00	$\pm 0.017 \dagger$	$\pm 0.17 / \pm 0.33$
BF			$\pm 0.10 \dagger$	± 1.00		± 1.00	$\pm 0.017 \dagger$	± 0.50
RF			$\pm 0.10 \dagger$	± 1.00		± 1.00	$\pm 0.017 \dagger$	± 0.33
BS			$\pm 0.10 \dagger$	± 0.50		± 1.00	$\pm 0.008 \dagger$	$\pm 0.10 \dagger$

tor) will be made by measuring and manufacturing an appropriate mount for each detector.

To evaluate image quality degradation after the tolerancing study, we isolated and analyzed the 90th

percentile of the Montecarlo simulations. (Hence we have a chance of 9 out of 10 to have a better image quality than this). The image quality is shown in Figure 7. Taking tolerances into account, the opti-

cal quality of the instrument remains within the requirements from Table 2. In the blue channel, band *g* achieves the requirements and goals inside a field of 5 arcmin in diameter, and the requirements in the whole area of the detector (including corners). In the red channel, bands *riz* achieve the goals in a field of 4.2 arcmin in diameter. The axial positions of the pupil planes shift from their nominal positions a maximum of ± 1 mm for the tip-tilt mirror and ± 0.5 mm for the deformable mirror. These are acceptable values to ensure the correct performance of the fast guiding and active optics systems.

7. THERMAL BEHAVIOR AND GHOSTS

COATLI will operate on Sierra San Pedro Mártir at an altitude of 2790 m with typical pressures of 0.72 atm. Temperatures throughout the year range from -15 to 30 C. The optics of COATLI have been designed at an intermediate temperature of 5 C. The optomechanics have been designed so that the optics will not move beyond the tolerances listed above in the given temperature range, and a detailed thermal analysis in Zemax has shown that the instrument can be compensated by focusing with the secondary mirror of the telescope and the deformable mirror, while not affecting the image quality.

We have analyzed light at the blue and red detectors coming from secondary reflections in all the optical components of the instrument using a Zemax non-sequential model. No ghosts were found at the blue detector. On the other hand, internal reflections in the red filters and the beam splitter produce ghosts at the red detector. However, these are approximately five orders of magnitude weaker than the primary image.

Masks will be placed at all intermediate focal planes (telescope's focal plane, pupil relay focal plane, before the blue filter wheel and before the red detector) and pupil planes (on the tip-tilt mirror and on the deformable mirror window), in order to reduce stray light.

8. FURTHER SCIENCE WITH THE B BAND

In addition to what has been presented, there are some scientific cases which require following stars in the *B* band, but do not need a very good image quality. The image quality in the design of COATLI in the *B* band is significantly worse than in the *g* band due to chromatic aberration, and the instrument has not been optimized for the *B* band. However, we have checked that the image quality in the *B* band is acceptable by refocusing with the telescope's

secondary mirror, delivering a FWHM better than 0.75 arcsec inside a field of view of 5 arcmin.

9. CONCLUSIONS

COATLI will produce images at the diffraction limit of a small telescope in the visible, in a wide field of view (4 arcmin) and in a relatively broad spectral range (550 to 920 nm), even in relatively poor seeing, with the only drawback of the telescope being relatively small (50 cm in diameter). In these terms, while being based on a standard collimator-camera system using lens systems, the optical design has no precedent in astronomical instrumentation. The solution that we present here is compact, low-risk, and offers an excellent performance.

The authors would like to thank all the COATLI project members, with special thanks to Carlos Tejada for very useful comments regarding the optical design. All lens polishing will be done at the IA-UNAM workshops by Oscar Chapa and Luis Carlos Álvarez. The dichroic, filters, and anti-reflecting coatings are provided by Custom Scientific. COATLI has been funded by the Instituto de Astronomía of the UNAM, CONACYT proposals 232649, 260369, and 271117 (Laboratorio Nacional de Astrofísica en San Pedro Mártir), and UNAM/PAPIIT projects IG100414 and IT102715.

REFERENCES

- Arsenault, R., Salmon, D., Kerr, J., et al. 1994, SPIE, 2201, 833
- Brown, W. R., Epps, H. W., & Fabricant, D. G. 2004, PASP, 116, 833
- Cuevas, S., López, J. A., Eikenberry, S., et al. 2006, NewAR, 50, 389
- Cuevas, S., Langarica, R., Watson, A. M., et al. 2016, SPIE, 9908, 5
- Gavel, D. T., Olivier, S. S., Bauman, B., Max, C. E. & Macintosh, B. 2000, SPIE, 4007, 63
- Hayward, T. L., Brandl, B., Pirger, B., et al. 2001, PASP, 113, 105
- Kopon, D., Close, L. M., Males, J., Gasho, V., & Follette, K. 2010, SPIE, 7736, 60
- Rousset, G., Lacombe, F., Puget, P., et al. 1998, SPIE, 3353, 508
- Skidmore, W., Els, S., Travouillon, T., et al. 2009, PASP, 121, 1151
- Tokovinin, A. & Heathcote, S. 2006, PASP, 118, 165
- Watson, A. M., Cuevas, S., Álvarez, L. C., et al. 2016, SPIE, 9908, 5
- Wilson, R. N. 2007, Reflecting Telescope Optics I, (Wilson Berlin: Springer)

J. Fuentes-Fernández, S. Cuevas, and A. M. Watson: Instituto de Astronomía, Ciudad Universitaria, UNAM, 04510 Ciudad de México, México (jfuentes@astro.unam.mx).